Electrical Control of Magnetic Phase Transition in a Type-I Multiferroic Double-Metal Trihalide Monolayer

Meiling Xu, Chengxi Huang, Yinwei Li, Siyu Liu, Xin Zhong, Puru Jena, Erjun Kan, and Yanchao Wang

Phys. Rev. Lett. **124**, 067602 — Published 14 February 2020

DOI: 10.1103/PhysRevLett.124.067602

Electrical Control of Magnetic Phase Transition in a Type-I Multiferroic Double-metal Trihalides Monolayer

Meiling Xu[1,⊥], Chengxi Huang[2,3,⊥], Yinwei Li[1,*], Siyu Liu[4], Xin Zhong[5], Puru Jena[3], Erjun Kan[2,†], and Yanchao Wang[4,‡]

[1]*School of Physics and Electronic Engineering, Jiangsu Normal University, Xuzhou 221116, China*

[2]*Department of Applied Physics and Institution of Energy and Microstructure, Nanjing University of Science and Technology, Nanjing, Jiangsu 210094, China*

[3]*Physics Department, Virginia Commonwealth University, Richmond, VA 23284*

[4]*State Key Lab of Superhard Materials & Innovation center of computational physics methods and software, College of Physics, Jilin University, Changchun 130012, China*

[5]*Key Laboratory of Functional Materials Physics and Chemistry of the Ministry of Education, Jilin Normal University, Changchun 130103, China*

Controlling magnetism of two-dimensional (2D) multiferroics by external electric field provides special opportunities both for fundamental research and future development of low-cost electronic nano-devices. Here, we report a general scheme for realizing magnetic-phase transition in 2D type-I multiferroic systems through the reversal of ferroelectric polarization. Based on first-principles calculations, we demonstrate that a single-phase 2D multiferroic, namely $ReWCl_6$ monolayer, exhibits two different low-symmetric (C_2) phases with opposite in-plane electric polarization and different magnetic order. As a result, an antiferro-to-ferromagnetic phase transition can be realized by reversing the in-plane electric polarization through the application of an external electric field. These findings not only enrich the 2D multiferroic family, but also uncover a unique and general mechanism to control magnetism by electric field, thus stimulating experimental interest.

Magnetoelectric coupling, mediated by the manipulation of magnetization through electric field, has great potential in the field of spintronics, such as magnetocapacitors, high-performance information storage and processing devices [1,2]. Consequently, multiferroic materials exhibiting strong magnetoelectric properties are much desired, but are naturally scarce owing to the inherent exclusion between ferroelectricity and ferromagnetism [3,4]. Inspired by the recent progress in the field of two-dimensional (2D) ferroelectricity [5,6] and ferromagnetism [7–9], 2D multiferroic materials have attracted considearble attention [10–17]. However, a magnetic phase transition induced by the reversal of ferroelectric polarization has never been observed in any 2D multiferroics.

Generally, there are two kinds of interactions responsible for magnetoelectric coupling, namely, spin-orbital and spin-lattice interactions [18]. The former is usually observed in type-II multiferroics, where the electric polarization is induced by symmetry breaking caused by a certain magnetic order (e.g. spiral magnetic order [19]). On the other hand, type-I multiferroics have been widely studied because of their strong and robust magnetization/polarization. However, magnetoelectric effect dominated by the spin-lattice interaction in type-I multiferroics is usually quite weak because the electric dipoles and magnetic moments often originate from different ions. Although a single-phase type-I multiferroic, in which the electric dipoles and magnetic moments have the same source, has been demonstrated [16], it is still unclear how to couple the magnetic phases and ferroelectric polarizations in such multiferroics.

In this Letter, we propose a general mechanism for realizing electrical control of magnetism in 2D type-I multiferroic systems. That is, in a 2D ferroelectric (FE) compound with triangular lattice, for example, $ReWCl_6$ monolayer where the electric polarization is induced by charge and orbital ordering, the reversal of the in-plane ferroelectric polarization is accompanied by a magnetic phase transition. In this sense, an external proper electric field not only reverses the electric polarization but also changes the magnetic ordering of the system. Our first-principles calculations demonstrate that there are two inequivalent multiferroic phases of $ReWCl_6$ monolayer with C_2 symmetry (denoted as D-type and C-type phases in the following). The D-type phase is antiferromagnetic (AFM) and has an electric polarization along [1-10] orientation, whereas the C-type phase is ferromagnetic (FM) with an electric polarization along [-110] orientation. Thus, the electric polarization and the magnetic phases in $ReWCl_6$ monolayer can be simultaneously manipulated by an external electric field. This mechanism is also observed in other 2D multiferroic compounds, which confirms its generality.

Our first-principles calculations are based on the density functional theory (DFT) [20] as implemented in the Vienna *ab initio* simulations package (VASP) [21]. The core electrons are treated by the projector augmented-wave (PAW) approximation [22], and the exchange-correlation functional is given by the generalized gradient approximation parameterized by Perdew, Burke, and Ernzerhof (GGA-PBE) [23]. An effective Hubbard U=1 eV is added following Dudarev's method [24] for the Re-5*d* and W-5*d* orbitals. The plane-wave cutoff energy is set to 600 eV in all calculations, and the first Brillouin zone is sampled using a Γ-centered 12 × 12 × 1 Monkhorst-Pack grid [25]. All geometries are relaxed until residual forces are smaller than 10^{-3} eV/Å. The FE polarization is calculated using the Berry phase method [26]. The maximally localized Wannier functions (MLWFs) are constructed by using the wannier90 package [27]. The phonon dispersion is calculated using the finite displacement method, as implemented in the PHONOPY code [28].

A typical character of FE materials is the switching of spontaneous electric polarization by reversing the external electric field. Akin to the case of ferromagnetism, the measured hysteresis loop is usually recognized as a criterion for ferroelectricity in experiments. Theoretically, the FE switching is defined as a transition between two equivalent structural phases with opposite electric polarization. 2D transition metal trihalides, which can be easily exfoliated from their van der Waals bulk phases, have recently received much attention [7]. Additionally, most of these materials are intrinsically magnetic. Thus, 2D transition metal trihalides can be an ideal platform to study possible electric-field-induced magnetic phase transition. However, a spontaneous polarization in such triangular lattices is absent without breaking the inversion or rotational symmetry. For example, in a 2D triangular lattice consisting of one cation and one anion [Fig. 1], the in-plane electric polarization can only be induced by breaking the in-plane C_3 symmetry (e.g. by introducing a lateral displacement of the anion), resulting in two possible inequivalent C_2 phases (denoted as D-type and C-type) with opposite electric dipoles. This is quite different from previously studied 2D FE systems [5,11,29–36]. Moreover, due to the crystal field change casued by structural deformation, D-type and C-type phases may exhibit different kinds of on-site energy level splitting, leading to different orbital ordering. Consequently, different magnetic and electronic properties of D-type and C-type phases are expected. Therefore, by applying an external electric field to reverse the electric polarization of this system, a structural phase transition accompanied by significant changes of magnetic and electronic properties can be realized.

To break the inversion or rotational symmetry of a 2D triangular lattice, one of the ideal candidate systems is the bi-metallic trihalide monolayer, for example, $ReWCl_6$ monolayer [Fig. 2], in which the Re and W ions are distributed in two nested 2D triangular frameworks. Different alloyed configurations of $ReWCl_6$ have been considered, and the honeycomb-checkboard pattern [Fig. 2] is lower by at least 20 meV/metal in energy than the other considered patterns (Fig. S1 [37]). Different from typical non-polar transition metal trihalide monolayers (e.g. CrI_3) with D_{3d} symmetry, a remarkable structural distortion occurs in the honeycomb-checkboard $ReWCl_6$ monolayer, resulting in the reduction of crystal symmetry from D_3 to C_2. Two different distorted phases of C_2-$ReWCl_6$ (denoted as D-type and C-type) are observed, which agree well with the physical model discussed in Fig. 1. In the D-type phase, each two neighboring Re and W ions tend to form a Re-W ***dimer*** with a bond length of 2.585 Å, which is much smaller than the other Re-W distance (3.803 Å). On the other hand, in C-type, parallel …Re-W-Re-W… ***chains*** are observed with a Re-W bond length of 3.002 Å, which is smaller than those between chains (3.865 Å). Note that both D-type and C-type phases can be reproduced by the CALYPSO method [47,48]. The formation energies [defined as $E_f = (E_{ReWCl_6} - 6 \times \mu_{Cl} - \mu_{Re} - \mu_W)/8$, where E_{ReWCl_6} is the total energy and μ_{Re}, μ_W and μ_{Cl} are chemical potentials taken from hexagonal Re crystal, bcc W metal crystal, and gas phase Cl_2, respectively] of D-type and C-type are -0.68 and -0.64 eV/atom, respectively. The dynamical and thermal stabilities of D-type and C-type have been verified by phonon calculations (Fig. S2 [37]) and *ab initio* molecular dynamic simulations (Fig. S3 [37]), respectively. These results indicate that both D-type and C-type $ReWCl_6$ monolayers are experimentally feasible.

As shown in Fig. 2, D_3-$ReWCl_6$ is metallic while both D-type and C-type phases are semiconductors with indirect band gaps of 0.67 and 0.38 eV, respectively (1.68 and 1.26 eV at HSE06 [49] level). Such metal-semiconductor transition is caused by large structural distortion which splits the t_{2g} levels of transition metal ions. The spin-orbit coupling barely affects the electronic structures, and is ignored hereafter. Close inspection of the spin density and projected density of states (PDOS) of D-type and C-type (Fig. 3) shows that the spin charges are mainly localized around the W ions, and spin-polarization near the Fermi level is mainly contributed by the W-5*d* orbitals. The formal spin moment for W and Re ions are 1 and 0 μ_B, respectively. Such a small magnetization can be understood from the valence states for W and Re ions, which are +5 and +1,

respectively. In this case, the magnetic moment of 1 μ_B comes from W^{5+}-d^1 electrons. There is no noticeable spin-polarization on Re ions because the Re^{1+}-d^6 electrons fully occupy the Re-t_{2g} orbitals. Also, the rearrangement of W-t_{2g} orbitals under different structural distortions leads to different orbital orderings for D-type and C-type phases, as shown in Fig. 3. From the on-site *d* levels derived from the MLWFs [38] (Table SII and Fig. S5 [37]), we find that the d_{xz}, d_{yz} orbitals are lower in energy than the d_{xy} orbital in the D-type phase. Thus, the spin-polarization for D-type phase is mainly contributed by d_{xz}, d_{yz} orbitals. On the contrary, in the C-type phase, the spin-polarization is dominated by d_{xy} orbitals because the d_{xz} and d_{yz} orbitals are higher in energy than the d_{xy} orbital. These results coincide exactly with the PDOS as illustrated in Fig. 3. Additionally, one can see a large overlap between W-5*d* and Re-5*d* orbitals from the PDOS, different from other previously studied bi-metallic compounds where *d* orbitals of different transition metals are distinctly separated [50,51]. Besides, the electron localization function (Fig. S7 [37]) shows bonding-like behavior between the nearest neighboring Re and W ions. Thus, there could be strong direct interactions between Re and W ions in the C_2-$ReWCl_6$ monolayer becasue of the delocalization of 5*d* orbitals in comparison with the localized 3*d* orbitals. Such strong Re-W interaction may also be responsible for the large structural distortions and the formations of ***dimers*** and ***chains*** in C_2-$ReWCl_6$ monolayer.

Since the spin-polarization is mainly contributed by W ions, here we only consider the magnetic couplings between neighboring W ions. The spin Hamiltonian can be written as,

$$\hat{H} = -\sum_i \left(2J_1 \vec{S}_i \cdot \vec{S}_{i,1} + J_2 \vec{S}_i \cdot \vec{S}_{i,2}\right),$$

where J_1 denotes the exchange interaction along [100] and [010]orientations, and J_2 denotes that along the [110] orientation. The summation *i* runs over all the W sites. Subscripts *i*/1/2 are the site indices; *S* is the formal magnetic moment at the W site. By energy mapping analysis on the considered magnetic configurations (Fig. S8 [37]), the calculated J_1 and J_2 of the D-type phase are 2.00 and -1.00 meV, respectively. The positive and negative values represent AFM and FM couplings, respectively. The ground state of the D-type phase is found to be chain-AFM (see Fig. 4). On the contrary, the ground state of the C-type phase is FM with J_1 and J_2 of -1.75 and 0.75 meV, respectively (Fig. S8 [37]). The difference between J_1 and J_2 for each phase can be understood by realizing that the AFM direct-exchange interactions between 5*d* orbitals are sensitive to the W-W

distance. Thus, a shorter W-W distance will enhance the AFM couplings, while a longer one will favor FM couplings. For instance, in the D-type phase, the W-W distance along [100] orientation is 5.723 Å, shorter than that along [110] orientation (6.142 Å). Thus, the J_1 is AFM while the J_2 is FM. On the other hand, the difference between J_1 of the D-type and C-type phases can be understood by spin-lattice interaction. In the D-type phase, the AFM direct-exchange interaction is due to the occupied $d_{xz,yz}$ orbitals, whereas in the C-type phase, those are contributed by the occupied d_{xy} orbitals. From the PDOS, the bandwidth of $d_{xz,yz}$ orbitals is larger than that of d_{xy} orbitals, indicating that the AFM direct-exchange interactions between $d_{xz,yz}$ orbitals is stronger. Thus, the J_1 for the D-type phase is AFM, while it is FM for the C-type phase.

Magnetic anisotropy (MA) is examined by including the spin-orbit coupling (SOC). The easy axis for both the D-type and C-type phases is along [1-10] in-plane orientation (Table SIII [37]). The magnetocrystalline anisotropic energies of the D-type and C-type phases are 275 and 650 μeV/W (with respect to the out-of-plane hard axis), respectively, much larger than those of traditional metals such as Fe (1.4 μeV/Fe). Monte-Carlo (MC) simulations further show that the magnetic critical temperature for AFM D-type and FM C-type phases are ~21 and ~10 K, respectively. Although the C-type phase shows a small spin-frustration, the MC results show that the FM order is stable below the Curie temperature.

Because of the reduced C_2 symmetry, both D-type and C-type $ReWCl_6$ monolayers are expected to be electrically polar. Interestingly, our results show that the electric polarization for D-type and C-type phases are parallel to the c_2 axis and are opposite to each other. The in-plane spontaneous polarization of FE orders are calculated to be 0.87×10^{-10} (along [1-10] orientation) and 0.54×10^{-10} C/m (along [-110] orientation) for D-type and C-type, respectively. If we estimate the thickness of the monolayer to be 6 Å, which is normally the interlayer spacing in layered transition metal trihalides, the polarizations are 5.24 and 3.22 μC/cm^2, respectively (see Fig. S9 and for details [37]). These values are comparable to those of recently reported 2D FE SnSe, phosphorene [12,35,52], 2D multiferroic $(CrBr_3)_2Li$ [16] and traditional bulk FE $BaTiO_3$ [53–55]. Different from previously studied 2D FE systems such as SnTe, In_2Se_3 and $CrBr_3$ [5,16,31,56], we find that the polarization of D-type or C-type phase can only be switched by 120° or 240° by adjusting the distance between neighboring W and Re ions. But for 180° FE switching, one has to interchange the positions of W and Re ions or rotate the whole structure by 60°, which is impossible by applying an external electric

field. What will happen if we reverse the external electric field, e.g. from [1-10] to [-110] direction? One possibility is a phase transition from the D-type to the C-type phase since they have opposite polarizations. This is confirmed by applying an in-plane homogeneous electric field (Section X in [37]).

The transition between the D-type and C-type phases was investigated by using the nudged elastic band (NEB) method (Fig. 4). All the intermediated states have in-plane polarization along the c_2 axis. The reversal of polarization occurs around the transition state whose structure is close to the D_3-$ReWCl_6$. The activation energy barrier from the D-type (C-type) to C-type (D-type) is ~0.53 (~0.21) eV/f.u., indicating that the coercive fields needed to switch the polarization along [1-10] and [-110] orientations could be different, leading to an asymmetric hysteresis. We also have explored the normal 120° FE switching of the D-type ground state (Fig. S10 [37]). The switching barrier is estimated to be ~0.32 eV/f.u., comparable to that of other 2D multiferroic materials [12,15,17,31,57]. This indicates that the FE order can be stable at high temperature.

Next, we study the magnetoelectric coupling effect. Because the D-type phase monolayer is AFM and has an electric polarization along [1-10] orientation, whereas the C-type phase is FM and has an electric polarization along [-110] orientation, the electric polarization and the magnetic phases in $ReWCl_6$ monolayer are coupled and are simultaneously tunable by an external electric field. The estimated magnetoelectric coupling coefficient is comparable to that of $Fe/BaTiO_3$ multiferroic interface (see section IX in [37]). Additionally, the band gap and effective mass for the D-type and C-type phases are also different (Fig. 2b), which are also controllable by an external electric field. We have also examined the strain effect on the $ReWCl_6$ monolayer (Fig. S4 [37]). The results show that an in-plane tensile biaxial strain may cause a phase transition from the D-type to the C-type phase. These findings will be useful for multi-functional spintronic applications.

It is now necessary to examine whether the inherent properties of 2D materials could be robust on substrates. Here, a nonmagnetic nonpolar insulator of SiO_2 slabs is chosen to support the $ReWCl_6$ monolayer. After careful optimization, no strong chemical bonds are formed between $ReWCl_6$ monolayer and the SiO_2 substrate, and the magnetic and electronic properties of isolated $ReWCl_6$ can be well-retained on substrates (see Fig. S11 for details [37]).

Finally, we discuss the generality of the explored mechanism by studying other ABX_6 (A and B are different transition metals) monolayers. We first adopt a tight-binding cluster model to study the

origin of coexistence of the D-type and C-type phases and the transitions between them (see Section VI [37]). The results show that the relative stability of the D-type and C-type phases is closely related to the inter-atomic exchange interactions between neighboring metal sites. A stronger inter-atomic exchange interaction will stabilize the D-type phase, whereas a weaker one favors the C-type phase. This explains the strain-induced phase transition between D-type and C-type phases (Fig. S4 [37]). On the basis of DFT calculations, we found that other ABX_6 systems, i.e. $ReWBr_6$ and $ReMoCl_6$, also exhibit similar phase-dependent magnetic and ferroelectric properties as $ReWCl_6$ (see section VIII [37]), where an electrical control of magnetic phase transition is also expected. These results demonstrate that the electrical control of magnetic phase transition and magnetoelectric effects are general phenomena in ABX_6 systems.

In summary, based on an unusual FE switching phenomenon, we propose a general strategy to realize electrical control of magnetic phase transition in 2D multiferroic materials. Through first-principles calculations, we discovered that the $ReWCl_6$ monolayer is a 2D multiferroic material, which possesses two possible inequivalent structural phases with opposite electric polarizations and different magnetic order. Thus, the transition between AFM and FM phases of $ReWCl_6$ monolayer can be tuned by applying a proper electric field, which also reverses the in-plane polarization. Similar magnetoelectric coupling effects are also found in other ABX_6 systems. These findings reveal a new mechanism of magnetoelectric coupling of electrical control of magnetic phase transition in 2D multiferroic materials, which is likely to create a great interest in future spintronic studies and applications.

We are supported by the National Natural Science Foundation of China under Grant Nos. 11774127, 11822404, 11722433, 11774173, 51790492, and 11904142. The computational resources have been provided by the High Performance Computing Center of the School of Physics and Electronic Engineering of Jiangsu Normal University. P. J. acknowledges support of the U.S DOE, Office of Basic Energy Sciences, Division of Material Sciences and Engineering under Award No. DE-FG02-96ER45579.

[⊥]M. X. and C. H. contributed equally to this work.

To whom all correspondence should be addressed.

[*]yinwei_li@jsnu.edu.cn

†ekan@njust.edu.cn

‡wyc@calypso.cn

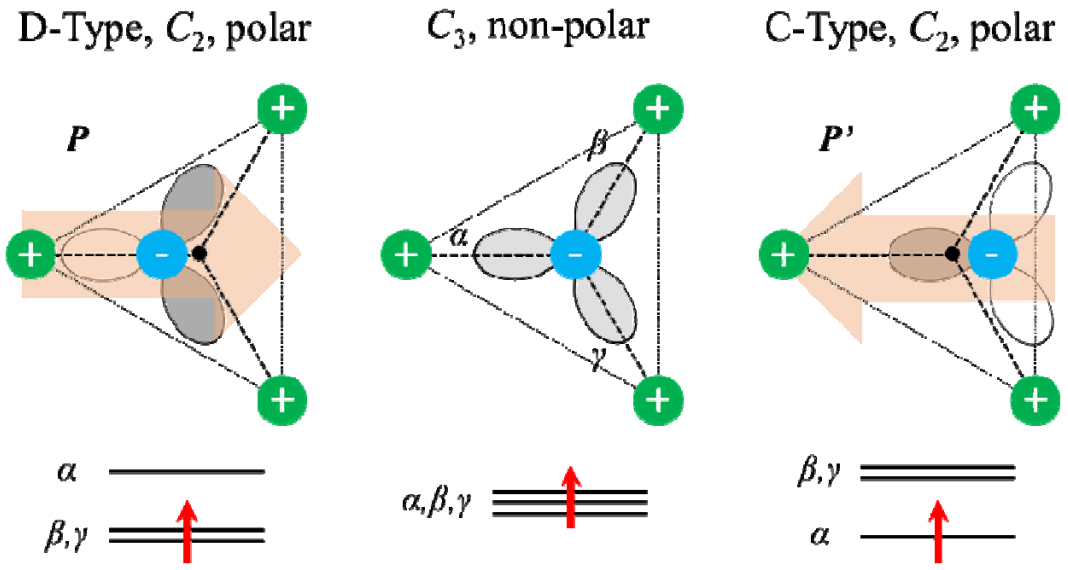

Figure 1. Schematic diagram of 180° FE switching and structure-mediated magnetoelectric effect in a 2D triangular lattice. "+" and "-" signs represent positive and negative charged ions. Orange arrows represent electric polarization. Red arrows represent spins. The oval shapes represent α, β and γ molecular orbitals, in which a darker color indicates a more occupied orbital.

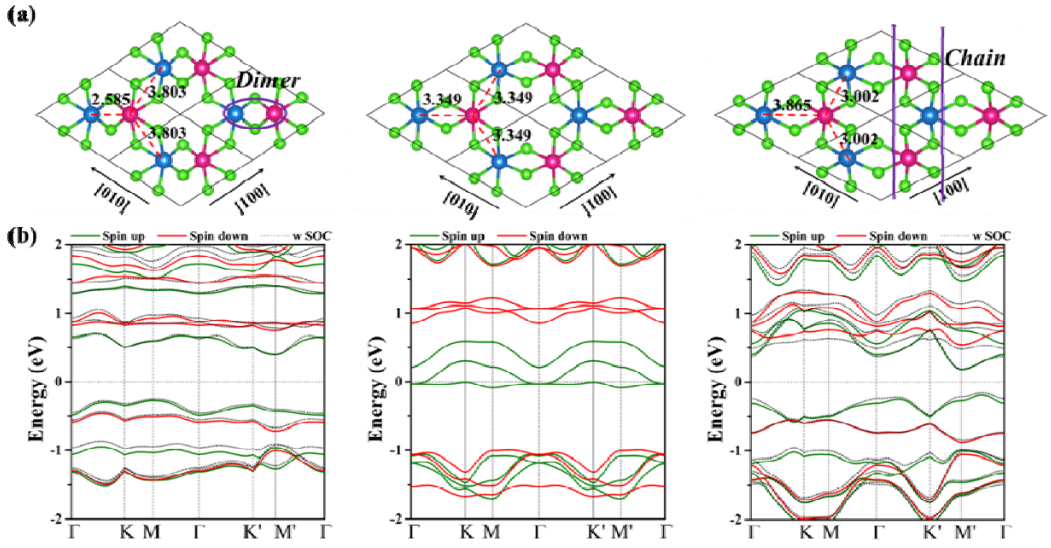

Figure 2. (a) Top views of the optimized structures and (b) electronic band structures of D-type, D_3, and C-type phases (from left to right), respectively, of $ReWCl_6$ monolayer. Re-W ***dimers*** and …Re-W-Re-W… ***chains*** are marked. Blue and red spheres represent W and Re atoms, respectively. Green and red curves denote the spin-up and spin-down bands, respectively. Dash black lines represent bands including SOC effect. The Fermi level is set to zero. The high symmetry points of the Brillouin zone can be found in Fig. S6 [37].

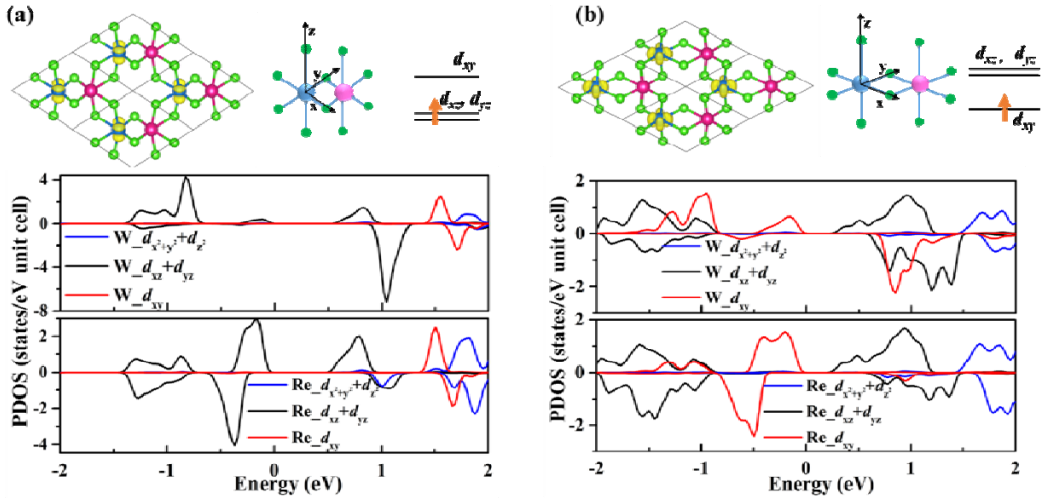

Figure 3. Spin density, on-site energy levels of W-t_{2g} orbitals (upper panel), and projected density of states (bottom panel) for (a) D-type and (b) C-type $ReWCl_6$ monolayer.

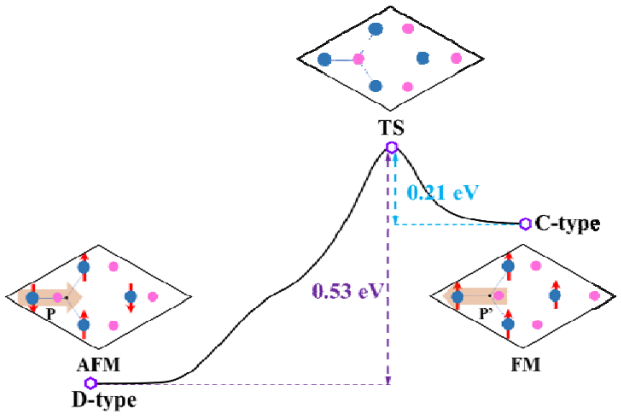

Figure 4. Kinetic pathway of phase transition process between D-type and C-type phases of $ReWCl_6$ monolayer. Blue and pink spheres represent W and Re atoms, respectively. Orange arrows represent the electric polarizations.

"↑" and "↓" arrows illustrate spin moments.

References

[1] W. Eerenstein, N. D. Mathur, and J. F. Scott, Nature **442**, 759 (2006).

[2] M. M. Vopson, Crit. Rev. Solid State Mater. Sci. **40**, 223 (2015).

[3] K. F. Wang, J.-M. Liu, and Z. F. Ren, Adv. Phys. **58**, 321 (2009).

[4] N. A. Spaldin, S.-W. Cheong, and R. Ramesh, Phys. Today **63**, 38 (2010).

[5] K. Chang, J. Liu, H. Lin, N. Wang, K. Zhao, A. Zhang, F. Jin, Y. Zhong, X. Hu, W. Duan, Q. Zhang, L. Fu, Q.-K. Xue, X. Chen, and S.-H. Ji, Science **353**, 274 (2016).

[6] J. Xiao, H. Zhu, Y. Wang, W. Feng, Y. Hu, A. Dasgupta, Y. Han, Y. Wang, D. A. Muller, L. W. Martin, P. A. Hu, and X. Zhang, Phys. Rev. Lett. **120**, 227601 (2018).

[7] B. Huang, G. Clark, E. Navarro-Moratalla, D. R. Klein, R. Cheng, K. L. Seyler, D. Zhong, E. Schmidgall, M. A. McGuire, D. H. Cobden, W. Yao, D. Xiao, P. Jarillo-Herrero, and X. Xu, Nature **546**, 270 (2017).

[8] C. Gong, L. Li, Z. Li, H. Ji, A. Stern, Y. Xia, T. Cao, W. Bao, C. Wang, Y. Wang, Z. Q. Qiu, R. J. Cava, S. G. Louie, J. Xia, and X. Zhang, Nature **546**, 265 (2017).

[9] D. R. Klein, D. MacNeill, J. L. Lado, D. Soriano, E. Navarro-Moratalla, K. Watanabe, T. Taniguchi, S. Manni, P. Canfield, J. Fernández-Rossier, and P. Jarillo-Herrero, Science **360**, 1218 (2018).

[10] J. Zhang, S. Wu, Y. Shan, J. Guo, S. Yan, S. Xiao, C. Yang, J. Shen, J. Chen, L. Liu, and X. Wu, ACS Nano **13**, 2334 (2019).

[11] J. J. Zhang, L. Lin, Y. Zhang, M. Wu, B. I. Yakobson, and S. Dong, J. Am. Chem. Soc. **140**, 9768 (2018).

[12] M. Wu and X. C. Zeng, Nano Lett. **16**, 3236 (2016).

[13] M. Wu, J. D. Burton, E. Y. Tsymbal, X. C. Zeng, and P. Jena, J. Am. Chem. Soc. **134**, 14423 (2012).

[14] L. Li and M. Wu, ACS Nano **11**, 6382 (2017).

[15] Q. Yang, W. Xiong, L. Zhu, G. Gao, and M. Wu, J. Am. Chem. Soc. **139**, 11506 (2017).

[16] C. Huang, Y. Du, H. Wu, H. Xiang, K. Deng, and E. Kan, Phys. Rev. Lett. **120**, 147601 (2018).

[17] Z. Tu, M. Wu, and X. C. Zeng, J. Phys. Chem. Lett. **8**, 1973 (2017).

[18] S. Dong, J.-M. Liu, S.-W. Cheong, and Z. Ren, Adv. Phys. **64**, 519 (2015).

[19] H. J. Xiang, S. H. Wei, M. H. Whangbo, and J. L. F. Da Silva, Phys. Rev. Lett. **101**, 037209 (2008).

[20] W. Kohn and L. J. Sham, Phys. Rev. **140**, A1133 (1965).

[21] G. Kresse, J. Non. Cryst. Solids **192**–**193**, 222 (1995).

[22] P. E. Blöchl, Phys. Rev. B **50**, 17953 (1994).

[23] J. P. Perdew, K. Burke, and M. Ernzerhof, Phys. Rev. Lett. **77**, 3865 (1996).

[24] S. L. Dudarev, G. A. Botton, S. Y. Savrasov, C. J. Humphreys, and A. P. Sutton, Phys. Rev. B **57**, 1505 (1998).

[25] H. J. Monkhorst and J. D. Pack, Phys. Rev. B **13**, 5188 (1976).

[26] R. D. King-Smith and D. Vanderbilt, Phys. Rev. B **47**, 1651 (1993).

[27] A. A. Mostofi, J. R. Yates, G. Pizzi, Y.-S. Lee, I. Souza, D. Vanderbilt, and N. Marzari, Comput. Phys. Commun. **185**, 2309 (2014).

[28] K. Parlinski, Z. Q. Li, and Y. Kawazoe, Phys. Rev. Lett. **78**, 4063 (1997).

[29] E. Kan, F. Wu, K. Deng, and W. Tang, Appl. Phys. Lett. **103**, 193103 (2013).

[30] S. N. Shirodkar and U. V. Waghmare, Phys. Rev. Lett. **112**, 157601 (2014).

[31] W. Ding, J. Zhu, Z. Wang, Y. Gao, D. Xiao, Y. Gu, Z. Zhang, and W. Zhu, Nat. Commun. **8**, 14956 (2017).

[32] F. Liu, L. You, K. L. Seyler, X. Li, P. Yu, J. Lin, X. Wang, J. Zhou, H. Wang, H. He, S. T. Pantelides, W. Zhou, P. Sharma, X. Xu, P. M. Ajayan, J. Wang, and Z. Liu, Nat. Commun. **7**, 12357 (2016).

[33] M. Wu, S. Dong, K. Yao, J. Liu, and X. C. Zeng, Nano Lett. **16**, 7309 (2016).

[34] A. Chandrasekaran, A. Mishra, and A. K. Singh, Nano Lett. **17**, 3290 (2017).

[35] R. Fei, W. Kang, and L. Yang, Phys. Rev. Lett. **117**, 097601 (2016).

[36] H. Tan, M. Li, H. Liu, Z. Liu, Y. Li, and W. Duan, Phys. Rev. B **99**, 195434 (2019).

[37] Supplemental Material includes refs. [38-46] for the relative energies of D-type and C-type phases considering Hubbard U effect, relative energies of different alloyed phases, phonon spectras, AIMD simulations, strain effects, MLWFs results, 2D Brillouin zone and corresponding high symmetric paths, electron localization function results, exchange

parameters, magnetocrystalline anisotropic energy, details for electric polarizations calculations, NEB results for FE swithcing of D-type phase, substrate effect, the tight binding cluster model, electrical control of magnetic phase transition in other ABX_6 systems, structural information for D-type and C-type phases, the magnetoelectric coupling coefficient and effect of external in-plane electric field.

[38] A. A. Mostofi, J. R. Yates, G. Pizzi, Y.-S. Lee, I. Souza, D. Vanderbilt, and N. Marzari, Comput. Phys. Commun. 185, 2309 (2014).

[39] C. Huang, J. Feng, J. Zhou, H. Xiang, K. Deng, and E. Kan, J. Am. Chem. Soc. 141, 12413 (2019).

[40] H. Katsura, N. Nagaosa, and A. V. Balatsky, Phys. Rev. Lett. 95, 057205 (2005).

[41] J. C. Slater and G. F. Koster, Phys. Rev. 94, 1498 (1954).

[42] C.-G. Duan, S. S. Jaswal, and E. Y. Tsymbal, Phys. Rev. Lett. 97, 047201 (2006).

[43] B. Xu, V. Garcia, S. Fusil, M. Bibes, and L. Bellaiche, Phys. Rev. B 95, 104104 (2017).

[44] T. Choi, Y. Horibe, H.T. Yi, Y.J. Choi, W. Wu, and S.-W. Cheong, Nat. Mater. **9**, 253 (2010).

[45] W. Ding, J. Zhu, Z. Wang, Y. Gao, D. Xiao, Y. Gu, Z. Zhang, and W. Zhu, Nat. Commun. 8, 14956 (2017).

[46] R. W. Nunes and X. Gonze, Phys. Rev. B 63, 155107 (2001).

[47] Y. Wang, J. Lv, L. Zhu, and Y. Ma, Comput. Phys. Commun. **183**, 2063 (2012).

[48] Y. Wang, J. Lv, L. Zhu, and Y. Ma, Phys. Rev. B **82**, 094116 (2010).

[49] J. Heyd, G. E. Scuseria, and M. Ernzerhof, J. Chem. Phys. **118**, 8207 (2003).

[50] C. Huang, J. Feng, F. Wu, D. Ahmed, B. Huang, H. Xiang, K. Deng, and E. Kan, J. Am. Chem. Soc. **140**, 11519 (2018).

[51] P. Zhou, C. Q. Sun, and L. Z. Sun, Nano Lett. **16**, 6325 (2016).

[52] T. Hu, H. Wu, H. Zeng, K. Deng, and E. Kan, Nano Lett. **16**, 8015 (2016).

[53] K. J. Choi, Science **306**, 1005 (2004).

[54] X. Wu, K. M. Rabe, and D. Vanderbilt, Phys. Rev. B **83**, 020104(R) (2011).

[55] J. C. Wojdeł and J. Íñiguez, Phys. Rev. B **90**, 014105 (2014).

[56] Y. Zhou, D. Wu, Y. Zhu, Y. Cho, Q. He, X. Yang, K. Herrera, Z. Chu, Y. Han, M. C. Downer, H. Peng, and K. Lai, Nano Lett. **17**, 5508 (2017).

[57] F Z. Zhu, X. Chen, W. Li, and J. Qi, Appl. Phys. Lett. **114**, 223102 (2019).